

# Probing transition form factors in the rare $B \rightarrow K^* \nu \bar{\nu}$ decay

Mohammad Ahmady,<sup>\*</sup> Alexandre Leger,<sup>†</sup> Zoe McIntyre,<sup>‡</sup> and Alexander Morrison<sup>§</sup>

*Department of Physics, Mount Allison University,  
Sackville, New Brunswick, Canada, E4L 1E6*

Ruben Sandapen<sup>¶</sup>

*Department of Physics, Acadia University,  
Wolfville, Nova-Scotia, Canada, B4P 2R6 and  
Department of Physics, Mount Allison University,  
Sackville, New Brunswick, Canada, E4L 1E6*

We compare the Standard Model (SM) predictions for the differential branching ratio of the rare  $B \rightarrow K^* \nu \bar{\nu}$  decays using  $B \rightarrow K^*$  form factors obtained from holographic light-front QCD (LFHQCD) and Sum Rules (SR) Distribution Amplitudes. For the total branching ratio, we predict  $\mathcal{BR}(B \rightarrow K^* \nu \bar{\nu})_{\text{LFHQCD}} = (6.36^{+0.59}_{-0.74}) \times 10^{-6}$  and  $\mathcal{BR}(B \rightarrow K^* \nu \bar{\nu})_{\text{SR}} = (8.14^{+0.16}_{-0.17}) \times 10^{-6}$ . More interestingly, we find that the two model predictions for the differential branching ratio are sufficiently different at low momentum transfer, so that future measurements at Belle II may be able to discriminate between them. We also confirm numerically that the  $K^*$  longitudinal polarization fraction  $F_L$  has little sensitivity to the non-perturbative form factors and is thus an excellent observable to probe New Physics signals. We predict  $F_L = 0.40^{+0.02}_{-0.01}(0.41 \pm 0.01)$  using LFHQCD (SR).

---

<sup>\*</sup> mahmady@mta.ca

<sup>†</sup> azleger@mta.ca

<sup>‡</sup> zxmccintyre@mta.ca

<sup>§</sup> ahmorrison@mta.ca

<sup>¶</sup> ruben.sandapen@acadiau.ca

## I. INTRODUCTION

The flavor changing neutral current (FCNC)  $b \rightarrow s$  transition has been at the focus of extensive experimental and theoretical investigations. This is due to the fact that, among other things, this rare transition is sensitive to new physics (NP) beyond the Standard Model (SM). Many observables for the dileptonic  $B \rightarrow K^* \mu^+ \mu^-$  decay have already been measured and the precision of the experimental data is expected to improve significantly in the near future. On the other hand, the rare decay  $B \rightarrow K^* \nu \bar{\nu}$  has not yet been measured experimentally and it is challenging to do so, as both leptons are detector eluding neutrinos. Only the upper bounds on the branching ratio ( $\mathcal{BR}$ ) are known and the most ones are set by the Belle Collaboration [1]:

$$\begin{aligned}\mathcal{BR}(B^+ \rightarrow K^{*+} \nu \bar{\nu}) &< 4.0 \times 10^{-5} \quad (90\% \text{ CL}) \quad , \\ \mathcal{BR}(B^0 \rightarrow K^{*0} \nu \bar{\nu}) &< 5.5 \times 10^{-5} \quad (90\% \text{ CL}) \quad .\end{aligned}\tag{1}$$

With the advent of Super-B facilities, the prospects of measuring these branching ratios in the near future are good. The Belle-II experiment, with an integrated luminosity  $50 \text{ ab}^{-1}$  that is expected to be collected by 2023, a measurement of the SM  $\mathcal{BR}$ s with 30% precision is expected [2]. Therefore, it is appropriate to have a closer look at this decay in order to motivate and further guide experimental efforts to measure the  $\mathcal{BR}$ s and related observables. Theoretically, the presence of only one operator in the effective Hamiltonian for the  $b \rightarrow s \nu \bar{\nu}$  transition makes  $B \rightarrow K^* \nu \bar{\nu}$  much less susceptible to hadronic uncertainty due to sensitivity to a minimal number of form factors. Moreover, this decay process does not suffer from additional uncertainties beyond the form factors, such as those that plague the  $b \rightarrow s \ell^+ \ell^-$  transitions due to the breaking of factorization caused by photon exchange. Indeed, for the  $B \rightarrow K^* \nu \bar{\nu}$  transition, factorization holds exactly, so a measurement of the decay rate would allow in principle to measure the form factors. This distinction also leads to the fact that, in contrast to  $B \rightarrow K^* \mu^+ \mu^-$  decays, the isospin asymmetries of the decays with neutrinos in the final state vanish identically, so the branching ratio of the  $B^0$  and  $B^\pm$  decays only differ due to the lifetime differences, i.e.  $\mathcal{BR}(B^+ \rightarrow K^{*+} \nu \bar{\nu})/\mathcal{BR}(B^0 \rightarrow K^{*0} \nu \bar{\nu}) = \tau_{B^+}/\tau_{B^0}$  is valid in the SM and beyond.

In this paper, we calculate the differential  $\mathcal{BR}$  as well as the  $K^*$  longitudinal polarization fraction for  $B \rightarrow K^* \nu \bar{\nu}$  decay. The form factors parameterizing the  $B \rightarrow K^*$  hadronic

matrix elements are derived via light-cone sum rules (LCSR)<sup>1</sup> in which the required Distribution Amplitudes (DAs) for  $K^*$  are obtained from the holographic light-front wavefunctions (LFWFs) for vector mesons[3] and from QCD Sum Rules [4]. Successful predictions of diffractive  $\rho$  and  $\phi$  meson electro-production at HERA [5–10] using holographic LFWFs, motivates us to use these alternative DAs in our calculation of form factors[11, 12]. The  $B \rightarrow (\rho, K^*)$  transition form factors using holographic  $\rho$  and  $K^*$  DAs have previously been used to calculate the differential decay rate of semileptonic  $B \rightarrow \rho \ell \nu$ [13] and dileptonic  $B \rightarrow K^* \mu^+ \mu^-$ [3] as well as the isospin asymmetry [14] and resonance effects[15] in the latter decay. In [15], we also found that our predictions for  $\mathcal{BR}(B \rightarrow K^* \mu^+ \mu^-)$  are not very different at low-to-intermediate  $q^2$  when using SR or holographic DAs (see Fig 5 of [15]). We shall see that the situation is different for  $\mathcal{BR}(B \rightarrow K^* \nu \bar{\nu})$ .

## II. THE EFFECTIVE HAMILTONIAN

The effective Hamiltonian for FCNC transition  $b \rightarrow s \nu \bar{\nu}$  in the SM is given as[16]

$$\mathcal{H} = -\frac{4G_F}{\sqrt{2}} V_{tb} V_{ts}^* C_L \mathcal{O}_L + h.c. , \quad (2)$$

where the only contributing operator  $\mathcal{O}_L$  is defined as:

$$\mathcal{O}_L = \frac{e^2}{8\pi^2} (\bar{s} \gamma_\mu P_L b) (\bar{\nu} \gamma^\mu P_L \nu) , \quad (3)$$

where  $P_L = (1 - \gamma_5)/2$  is the left-handed projection operator and  $C_L$  is the Wilson coefficient given by

$$C_L = \frac{-X(x_t)}{s_w^2} , \quad (4)$$

with  $s_w^2 = \sin^2 \theta_w \sim 0.23$  ( $\theta_w$  is the weak angle) and  $x_t = m_t^2/m_W^2$ . The leading-order (LO) contributions to  $X(x_t)$  can be written as:

$$X_0(x_t) = C_0(x_t) - 4B_0(x_t) , \quad (5)$$

where the effective vertex functions  $B_0$  and  $C_0$  represent the box and penguin diagrams shown in Figure (1). Explicitly,

$$B_0(x) = \frac{x}{4(x-1)^2} \ln(x) - \frac{x}{4(x-1)} , \quad (6)$$

$$C_0(x) = \frac{3x^2 + 2x}{8(x-1)^2} \ln(x) + \frac{x^2 - 6x}{8(x-1)} . \quad (7)$$

---

<sup>1</sup> LCSR form factors are accurate for low-to-intermediate  $q^2$ .

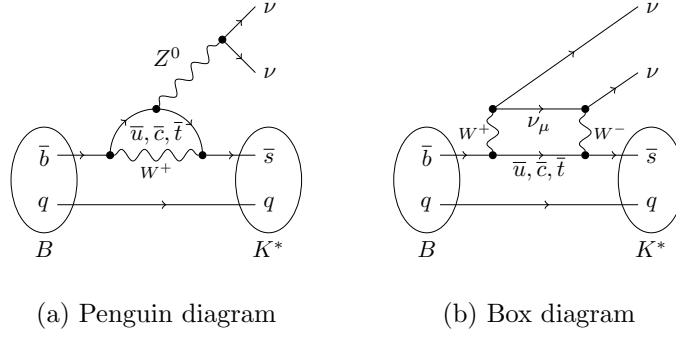


FIG. 1 Feynman diagrams of the principal contributions to the  $B \rightarrow K^* \nu \bar{\nu}$  decay.

Using  $m_t = 173.21 \pm 0.51 \pm 0.71$  GeV and  $m_W = 80.385 \pm 0.015$  GeV [17], one obtains  $X_0 = 1.59 \pm 0.01$  to LO. Including the next-to-leading order (NLO) QCD corrections along with the two-loop electroweak contributions reduces  $X_0$  by about 10% to  $X = 1.469 \pm 0.017$  [18–20].

The transition  $B \rightarrow K^*$  via the effective Hamiltonian given by Eq. (2) is parametrized by four form factors:

$$\begin{aligned}
 \langle K^*(k, \varepsilon) | \bar{s} \gamma^\mu (1 - \gamma^5) b | B(p) \rangle = & \frac{2iV(q^2)}{m_B + m_{K^*}} \epsilon^{\mu\nu\rho\sigma} \varepsilon_\nu^* k_\rho p_\sigma - 2m_{K^*} A_0(q^2) \frac{\varepsilon^* \cdot q}{q^2} q^\mu \\
 & - (m_B + m_{K^*}) A_1(q^2) \left( \varepsilon^{\mu*} - \frac{\varepsilon^* \cdot q q^\mu}{q^2} \right) \\
 & + A_2(q^2) \frac{\varepsilon^* \cdot q}{m_B + m_{K^*}} \left[ (p + k)^\mu - \frac{m_B^2 - m_{K^*}^2}{q^2} q^\mu \right], \quad (8)
 \end{aligned}$$

where  $\varepsilon$  is the polarization 4-vector of the  $K^*$ . The form factors  $A_0$ ,  $A_1$ ,  $A_2$  and  $V$  are sensitive to nonperturbative QCD and therefore one should resort to a specific model to calculate them. In a previous paper, we calculated  $B \rightarrow K^*$  transition form factors by using the light-cone sum rules (LCSR) along with holographic distribution amplitudes (DAs) obtained from holographic light-front QCD[3]. In this paper, we also estimate the uncertainty in the form factors resulting from the uncertainties due to quark masses.

### III. DISTRIBUTION AMPLITUDES FOR THE $K^*$

We now proceed to predict the twist-2 DAs  $\phi_{K^*}^{\parallel,\perp}(x, \mu)$  by writing them in terms of the light-front wavefunctions for  $K^*$  [21]:

$$f_{K^*} \phi_{K^*}^{\parallel}(x, \mu) = \sqrt{\frac{N_c}{\pi}} \int db \mu J_1(\mu b) \left[ 1 + \frac{m_{\bar{q}} m_s - \nabla_b^2}{M_{K^*}^2 x(1-x)} \right] \Psi_L(x, \zeta), \quad (9)$$

and

$$f_{K^*}^{\perp}(\mu) \phi_{K^*}^{\perp}(x, \mu) = \sqrt{\frac{N_c}{2\pi}} \int db \mu J_1(\mu b) [m_s - x(m_s - m_{\bar{q}})] \frac{\Psi_T(x, \zeta)}{x(1-x)}, \quad (10)$$

where  $f_{K^*}$  and  $f_{K^*}^{\perp}$  are the longitudinal and transverse coupling constants, respectively.  $\mu$  is the nonperturbative hadronic scale and the above expressions are valid at  $\mu \sim 1$  GeV, which is a scale representing transition from perturbative to non-perturbative regimes.  $\Psi_{\lambda}(x, \zeta)$  are holographic meson wavefunctions obtained by solving the holographic light-front Schrödinger Equation for mesons [22]. Explicitly,

$$\Psi_{\lambda}(x, \zeta) = \mathcal{N}_{\lambda} \sqrt{x(1-x)} \exp \left[ -\frac{\kappa^2 \zeta^2}{2} \right] \exp \left[ -\frac{(1-x)m_s^2 + x m_{\bar{q}}^2}{2\kappa^2 x(1-x)} \right], \quad (11)$$

where  $\lambda = L, T$  denotes the polarization and  $\zeta = \sqrt{x\bar{x}b}$  is the so-called holographic variable [22]. The polarization-dependent normalization constant  $\mathcal{N}_{\lambda}$  by requiring that [11]

$$\sum_{h, \bar{h}} \int d^2b dx |\Psi_{h, \bar{h}}^{K^*, \lambda}(x, b)|^2 = 1, \quad (12)$$

where the helicity-dependent wavefunctions in Eq. 12 are given by [12, 21]

$$\Psi_{h, \bar{h}}^{K^*, L}(x, b) = \frac{1}{2} \delta_{h, -\bar{h}} \left[ 1 + \frac{m_{\bar{q}} m_s - \nabla_b^2}{x(1-x) M_{K^*}^2} \right] \Psi_L(x, \zeta), \quad (13)$$

and

$$\Psi_{h, \bar{h}}^{K^*, T}(x, b) = \pm \left[ i e^{\pm i \theta_b} (x \delta_{h\pm, \bar{h}\mp} - (1-x) \delta_{h\mp, \bar{h}\pm}) \partial_b + [x m_{\bar{q}} + (1-x) m_s] \delta_{h\pm, \bar{h}\pm} \right] \frac{\Psi_T(x, \zeta)}{2x(1-x)}. \quad (14)$$

In Eq.(11),  $\kappa$  is the fundamental confinement scale [22] that emerges in light-front holography. Spectroscopic data indicate that  $\kappa = 0.55$  GeV for light vector mesons and a similar value,  $\kappa = 0.54$  GeV, is also favoured by the data for diffractive electroproduction of  $\rho$  and  $\phi$  vector mesons [11, 12]. We shall therefore use the latter value here. As for the quark masses  $m_{\bar{q}/s}$ , we shall fix them here in order to fit the experimentally measured decay constant  $f_{K^*}$

and we also check that our prediction for the ratio of transverse to longitudinal coupling,  $f_{K^*}^\perp/f_{K^*}$  is in reasonable agreement with lattice predictions.

The longitudinal and transverse couplings are given by [12, 21]

$$f_{K^*} = \sqrt{\frac{N_c}{\pi}} \int_0^1 dx \left[ 1 + \frac{m_{\bar{q}}m_s - \nabla_b^2}{x(1-x)M_{K^*}^2} \right] \Psi_L(\zeta, x)|_{\zeta=0} , \quad (15)$$

and

$$f_{K^*}^\perp(\mu) = \sqrt{\frac{N_c}{2\pi}} \int_0^1 dx (xm_{\bar{q}} + (1-x)m_s) \int db \mu J_1(\mu b) \frac{\Psi_T(\zeta, x)}{x(1-x)} , \quad (16)$$

respectively, which are obtained from the normalization condition on DAs, i.e.

$$\int \phi_{K^*}^{\parallel, \perp}(x, \mu) dx = 1 . \quad (17)$$

Our predictions are shown in Table I. As can be seen, different sets of quark masses can be used to fit the measured decay constant with the larger quark masses being preferred in order to approach the lattice data for the ratio  $f_{K^*}^\perp(\mu)/f_{K^*}$ . Guided by our predictions in Table I, we shall use  $m_{\bar{q}} = (195 \pm 55)$  MeV and  $m_s = (300 \pm 20)$  MeV in this paper.

Approach	Scale $\mu$	$m_{\bar{q}}$ [MeV]	$m_s$ [MeV]	$f_{K^*}$ [MeV]	$f_{K^*}^\perp(\mu)$ [MeV]	$f_{K^*}^\perp/f_{K^*}(\mu)$
LFHQCD	$\sim 1$ GeV	140	280	200	118	0.59
LFHQCD	$\sim 1$ GeV	195	300	200	132	0.66
LFHQCD	$\sim 1$ GeV	250	320	200	142	0.71
Experiment				$205 \pm 6^a$		
Lattice	2 GeV					$0.780 \pm 0.008$
Lattice	2 GeV					$0.74 \pm 0.02$

<sup>a</sup> From  $\Gamma(\tau^- \rightarrow K^{*-} \nu_\tau)$

TABLE I Comparison between LFHQCD predictions for the decay constant of the  $K^*$  meson with experiment [23], and the ratio of couplings with lattice [24, 25] data.

We can now compare the holographic DAs with those obtained using QCD Sum Rules. Note that Sum Rules predict the moments of the DAs:

$$\langle \xi_{\parallel, \perp}^n \rangle_\mu = \int dx \xi^n \phi_{K^*}^{\parallel, \perp}(x, \mu) \quad (18)$$

and that only the first two moments are available in the standard SR approach [26]. The twist-2 DA are then reconstructed as a Gegenbauer expansion

$$\phi_{K^*}^{\parallel,\perp}(x, \mu) = 6x\bar{x} \left\{ 1 + \sum_{j=1}^2 a_j^{\parallel,\perp}(\mu) C_j^{3/2}(2x-1) \right\}. \quad (19)$$

where  $C_j^{3/2}$  are the Gegenbauer polynomials and the coefficients  $a_j^{\parallel,\perp}(\mu)$  are related to the moments  $\langle \xi_{\parallel,\perp}^n \rangle_\mu$  [27]. These moments and coefficients are determined at a starting scale  $\mu = 1$  GeV and can then be evolved perturbatively to higher scales [26].

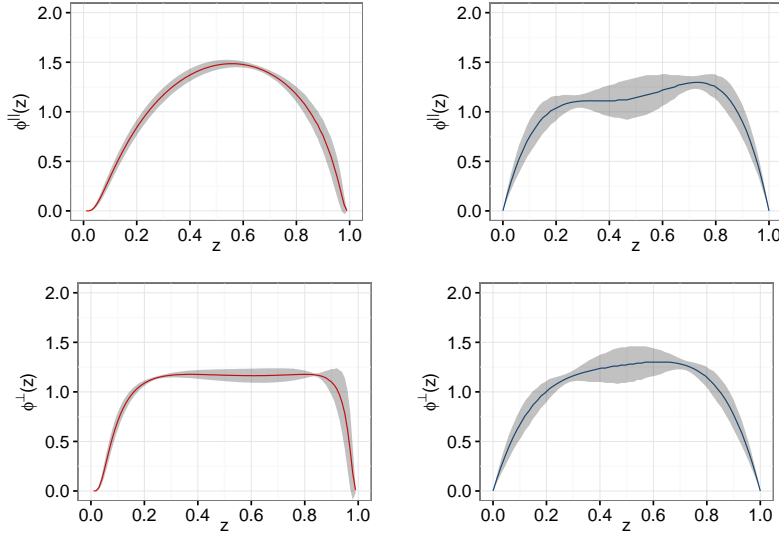


FIG. 2 Twist-2 DAs predicted by LFHQCD (graphs on the left) and SR (graphs on the right). The uncertainty band is due to the variation of the quark masses for AdS/QCD and the error bar on Gegenbauer coefficients for SR.

Figure 2 shows twist-2 DAs  $\phi^{\parallel,\perp}(z, \mu = 1 \text{ GeV})$  for the  $K^*$  vector meson obtained from Eqs. 9 and 10 as compared to SR predictions as given by Eq. 19. The uncertainty band for holographic DAs are due to different sets of  $(m_s, m_{\bar{q}})$  that fit the measured decay constant as shown in Table I. The error band in SR DAs are the result of the uncertainties in the Gegenbauer coefficients, ie.  $a_1^{\parallel} = 0.06 \pm 0.04$ ,  $a_2^{\parallel} = 0.16 \pm 0.09$  for  $\phi^{\parallel}(z, \mu = 1 \text{ GeV})$  and  $a_1^{\perp} = 0.04 \pm 0.03$ ,  $a_2^{\perp} = 0.10 \pm 0.08$  for  $\phi^{\perp}(z, \mu = 1 \text{ GeV})$  [4].

#### IV. $B \rightarrow K^*$ TRANSITION FORM FACTORS

As we noted before, the form factors, computed via LCSR, are valid at low to intermediate  $q^2$ . The extrapolation to high  $q^2$  is performed via a two-parameter fit of the following form

$$F(q^2) = \frac{F(0)}{1 - a(q^2/m_B^2) + b(q^4/m_B^4)} \quad (20)$$

to the LCSR predictions as well as form factor values obtained by the lattice QCD which are available at high  $q^2$ . The results for the above fit are summarized in Table II.  $A_{12}$  is a combination of the two form factors  $A_1$  and  $A_2$  which appears in the expression for the differential decay rate and is given as:

$$A_{12}(q^2) = \frac{(m_B + m_{K^*})^2(m_B^2 - m_{K^*}^2 - q^2)A_1(q^2) - \lambda_{K^*}(q^2)A_2(q^2)}{16m_B m_{K^*}^2(m_B + m_{K^*})}, \quad (21)$$

where  $\lambda_{K^*}$  is a kinematical factor and is given as the following:

$$\lambda_{K^*}(q^2) = m_B^4 + m_{K^*}^4 + q^4 - 2(m_B^2 m_{K^*}^2 + m_B^2 q^2 + m_{K^*}^2 q^2).$$

	F(0) (LFHQCD)	F(0) (SR)	a (LFHQCD)	a (SR)	b (LFHQCD)	b (SR)
$V$	$0.38^{+0.01}_{-0.03}$	$0.43 \pm 0.03$	$1.53^{+0.09}_{-0.05}$	$1.67^{+0.11}_{-0.10}$	$0.62^{+0.14}_{-0.12}$	$0.90^{+0.13}_{-0.11}$
$A_1$	$0.29^{+0.01}_{-0.02}$	$0.34 \pm 0.02$	$0.24^{+0.11}_{-0.06}$	$0.36 \pm 0.17$	$-0.68^{+0.18}_{-0.16}$	$-0.37 \pm 0.17$
$A_{12}$	$0.21 \pm 0.01$	$0.25 \pm 0.01$	$0.33^{+0.08}_{-0.07}$	$0.11^{+0.15}_{-0.14}$	$-0.56^{+0.16}_{-0.15}$	$-0.61 \pm 0.12$

TABLE II LFHQCD+ lattice prediction for the form factors. Lattice data is taken from [28]. The error bars for the holographic form factors are due to the variation of the quark masses as explained in the text.

Figures 3 shows the LFHQCD predictions including the lattice data points at high  $q^2$  for the form factors  $V$ ,  $A_1$  and  $A_{12}$ . The shaded bands in these figures represent the uncertainty due to the error band in the DAs. Note that there is an additional uncertainty in the form factors inherent in the LCSR method (uncertainty in the Borel parameter, continuum threshold and other input parameters). Since our goal in this paper is to discriminate between the LFHQCD and SR models and that the inherent LCSR uncertainties are the same in both models, we do not include them here. Table III shows the numerical values of the input parameters used in our predictions of the form factors and the decay rate.



$s_w^2$	0.23126(5)	$M_B$	8 GeV <sup>2</sup>
$\alpha$	127.925(16)	$s_0$	36 GeV <sup>2</sup>
$ V_{tb}V_{ts}^* $	0.0407(10)	$f_B$	0.18(1) GeV
$\tau_B$	1.519(5)ps	$m_b^{1S}$	4.60 GeV

TABLE III Numerical values of the input parameters.

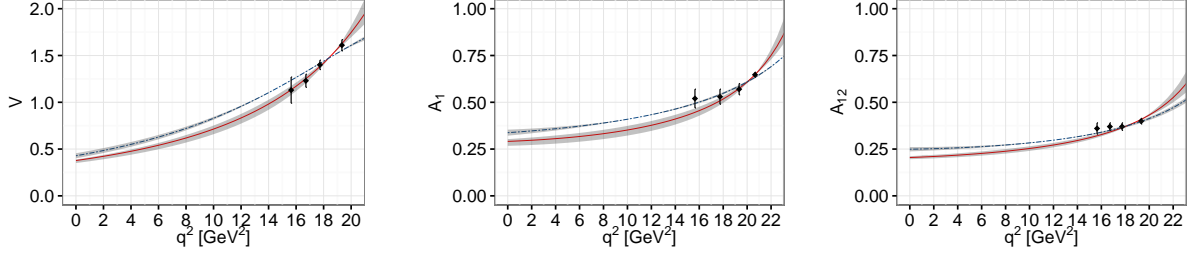


FIG. 3 LFHQCD predictions for the form factors  $V$ ,  $A_1$  and  $A_{12}$ . The two-parameter fits with the available lattice data (red) are shown and compared with the predictions of QCD SM (dashed blue). The shaded band represents the uncertainty in the predicted form factors due to uncertainty bands in DAs and variation in quark masses.

## V. DIFFERENTIAL DECAY RATE

Once the form factors are known, the differential branching ratio for  $B \rightarrow K^* \nu \bar{\nu}$  can be written as[16]:

$$\frac{d\mathcal{BR}(B \rightarrow K^* \nu \bar{\nu})}{dq^2} = \tau_B 3 |N|^2 \frac{X^2}{s_w^4} [\rho_{A_1}(q^2) + \rho_{A_{12}}(q^2) + \rho_V(q^2)], \quad (22)$$

where

$$N = V_{tb} V_{ts}^* \frac{G_F \alpha}{16\pi^2} \sqrt{\frac{m_B}{3\pi}},$$

and the functions  $\rho_V$ ,  $\rho_{A_1}$  and  $\rho_{A_{12}}$  are defined in terms of the form factors:

$$\rho_V(q^2) = \frac{2q^2 \lambda_{K^*}^{3/2}(q^2)}{(m_B + m_{K^*})^2 m_B^4} [V(q^2)]^2, \quad (23)$$

$$\rho_{A_1}(q^2) = \frac{2q^2 \lambda_{K^*}^{1/2}(q^2) (m_B + m_{K^*})^2}{m_B^4} [A_1(q^2)]^2, \quad (24)$$

$$\rho_{A_{12}}(q^2) = \frac{64 m_{K^*}^2 \lambda_{K^*}^{1/2}(q^2)}{m_B^2} [A_{12}(q^2)]^2. \quad (25)$$

Figure 4 compare the LFHQCD and SR predictions for the  $B \rightarrow K^* \nu \bar{\nu}$  differential decay rate. The resulting uncertainty due to form factors is shown as the shaded band. We observe that, in general, the LFHQCD prediction is lower than SR prediction for all values of the momentum transfer  $q^2$ . The difference between the two predictions is maximal ( $\sim 25\%$ ) for intermediate values of  $q^2$ . Most interestingly, the two predictions are quite distinct at low-to-intermediate  $q^2$  where LCSR method is most reliable. We expect that a future measurement of this decay channel at BELLE II may be able to discriminate between the two predictions. For the total branching ratio, we predict  $\mathcal{BR}(B \rightarrow K^* \nu \bar{\nu})_{\text{AdS/QCD}} = (6.36^{+0.59}_{-0.74}) \times 10^{-6}$ , compared to sum rules result  $\mathcal{BR}(B \rightarrow K^* \nu \bar{\nu})_{\text{SR}} = (8.14^{+0.16}_{-0.17}) \times 10^{-6}$ .

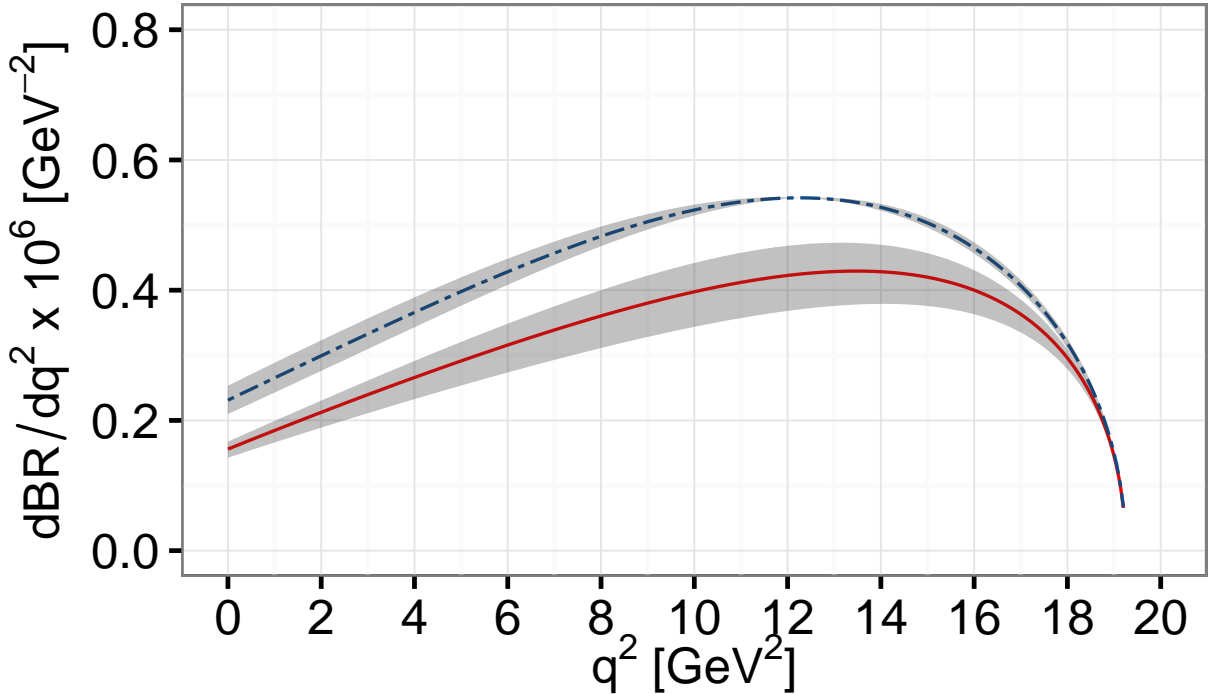


FIG. 4 The LFHQCD (Solid line) and SR (Dashed line) predictions for the differential Branching Ratio for  $B \rightarrow K^* \nu \bar{\nu}$ . The shaded band represents the uncertainty coming from the form factors.

The  $K^*$  longitudinal polarization fraction  $F_L$  is another observable associated with  $B \rightarrow K^* \nu \bar{\nu}$  decay. Indeed, within the SM, the branching ratio for B decay to longitudinal  $K^*$  and the neutrino-anti-neutrino pair is due to the second term in Eq. 22 and therefore,

for a given  $q^2$ , the fraction  $F_L$  can be written as [29]:

$$\frac{dF_L(B \rightarrow K^* \nu \bar{\nu})_{SM}}{dq^2} = \frac{\rho_{A_{12}}(q^2)}{\rho_{A_1}(q^2) + \rho_{A_{12}}(q^2) + \rho_V(q^2)} . \quad (26)$$

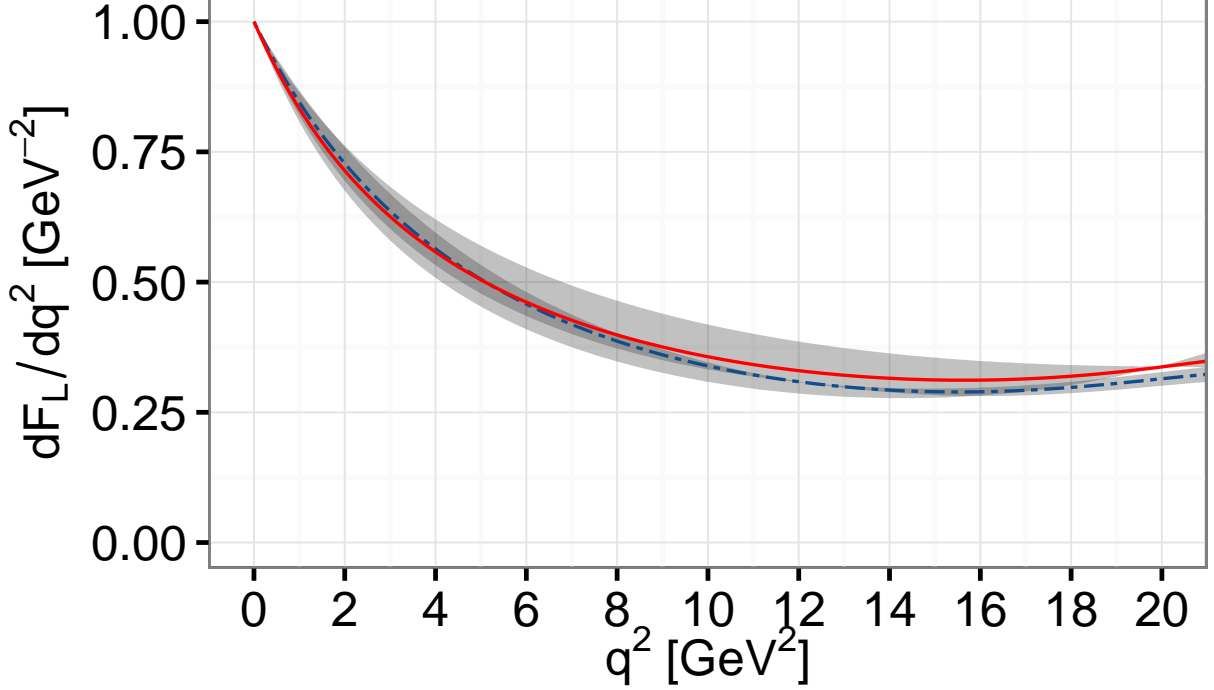


FIG. 5 The LFHQCD (Solid line) and SR (Dashed line) predictions for the polarization fraction distribution for  $B \rightarrow K^* \nu \bar{\nu}$ . The shaded band represents the uncertainty coming from the form factors.

Figure 5 shows our predictions for  $F_L$  versus  $q^2$ . We observe that within error bands, the two model predictions are not distinguishable. This confirms that the  $K^*$  longitudinal polarization fraction  $F_L$  has little sensitivity to the non-perturbative form factors and is thus an excellent observable to probe New Physics signals. Integrating over the whole kinematic region  $0 \leq q^2 \leq (m_B - m_{K^*})^2$ , we predict

$$F_L(B \rightarrow K^* \nu \bar{\nu})_{SM}^{LFHQCD} = 0.40^{+0.02}_{-0.01} , \quad (27)$$

as compared to  $F_L(B \rightarrow K^* \nu \bar{\nu})_{SM}^{SR} = 0.41 \pm 0.01$ .

In Table IV, we present bin-by bin predictions of LFHQCD and SR for the branching ratio and longitudinal polarization asymmetry. The predictions in a  $q^2$  bin  $[a, b]$  are computed using

$$\langle \mathcal{BR}_{K^*} \rangle \int_a^b \frac{d\mathcal{BR}(B \rightarrow K^* \nu \bar{\nu})}{dq^2} dq^2 , \quad (28)$$

and

$$\langle F_L \rangle \frac{\int_a^b \rho_{A_{12}}(q^2) dq^2}{\int_a^b (\rho_{A_1}(q^2) + \rho_{A_{12}}(q^2) + \rho_V(q^2)) dq^2} . \quad (29)$$

$q^2$	$10^6 \langle \mathcal{BR}^{LFHQCD} \rangle$	$10^6 \langle \mathcal{BR}^{SR} \rangle$	$\langle F_L^{LFHQCD} \rangle$	$\langle F_L^{SR} \rangle$
0 – 4	$0.85^{+0.07}_{-0.10}$	$1.20 \pm 0.09$	$0.71^{+0.002}_{-0.01}$	$0.73 \pm 0.01$
4 – 8	$1.26^{+0.13}_{-0.17}$	$1.71 \pm 0.08$	$0.46^{+0.02}_{-0.01}$	$0.46 \pm 0.01$
8 – 12	$1.58^{+0.18}_{-0.21}$	$2.08 \pm 0.03$	$0.35^{+0.02}_{-0.01}$	$0.35 \pm 0.01$
12 – 16	$1.69^{+0.16}_{-0.19}$	$2.08 \pm 0.02$	$0.32 \pm 0.01$	$0.30 \pm 0.01$
16 – $max$	$0.97 \pm 0.06$	$1.08^{+0.02}_{-0.03}$	$0.32 \pm 0.01$	$0.30 \pm 0.01$
0 – $max$	$6.36^{+0.59}_{-0.74}$	$8.14^{+0.16}_{-0.17}$	$0.40^{+0.02}_{-0.01}$	$0.41 \pm 0.01$

TABLE IV Bin-by-bin LFHQCD and SR predictions for the branching ratio and longitudinal polarization asymmetry.

## VI. CONCLUSION

Experimental observation of  $B \rightarrow K^* \nu \bar{\nu}$  can provide an excellent probe for the theoretical  $B \rightarrow K^*$  transition form factors. The differential branching ratio for this decay shows the largest sensitivity to the form factors for low-to-intermediate values of the momentum transfer. The  $K^*$  longitudinal polarization fraction, on the other hand, is not sensitive to the form factors, which makes it an interesting observable for NP search.

## VII. ACKNOWLEDGEMENT

M. A. and R. S. are supported by individual Discovery Grants from the Natural Sciences and Engineering Research Council of Canada (NSERC): No. SAPIN-2017-00033 and No. SAPIN-2017-00031, respectively. We thank Michael Thibodeau for his input in coding.

- 
- [1] O. Lutz et al. (Belle), Phys. Rev. **D87**, 111103 (2013), 1303.3719.  
[2] T. Aushev et al. (2010), 1002.5012.

- [3] M. Ahmady, R. Campbell, S. Lord, and R. Sandapen, Phys. Rev. **D89**, 074021 (2014), 1401.6707.
- [4] A. Bharucha, D. M. Straub, and R. Zwicky, JHEP **08**, 098 (2016), 1503.05534.
- [5] C. Adloff et al. (H1), Eur. Phys. J. **C13**, 371 (2000), hep-ex/9902019.
- [6] S. Aid et al. (H1), Nucl. Phys. **B463**, 3 (1996), hep-ex/9601004.
- [7] J. Breitweg et al. (ZEUS), Eur. Phys. J. **C2**, 247 (1998), hep-ex/9712020.
- [8] S. Chekanov et al. (ZEUS), Nucl. Phys. **B718**, 3 (2005), hep-ex/0504010.
- [9] The H1 Collaboration, JHEP **05**, 032 (2010), 0910.5831.
- [10] S. Chekanov et al. (ZEUS), PMC Phys. **A1**, 6 (2007), 0708.1478.
- [11] J. R. Forshaw and R. Sandapen, Phys.Rev.Lett. **109**, 081601 (2012), 1203.6088.
- [12] M. Ahmady, R. Sandapen, and N. Sharma, Phys. Rev. **D94**, 074018 (2016), 1605.07665.
- [13] M. Ahmady, R. Campbell, S. Lord, and R. Sandapen, Phys. Rev. **D88**, 074031 (2013), 1308.3694.
- [14] M. Ahmady, S. Lord, and R. Sandapen, Phys.Rev. **D90**, 074010 (2014), 1407.6700.
- [15] M. Ahmady, D. Hatfield, S. Lord, and R. Sandapen, Phys. Rev. **D92**, 114028 (2015), 1508.02327.
- [16] A. J. Buras, J. Girrbach-Noe, C. Niehoff, and D. M. Straub, JHEP **02**, 184 (2015), 1409.4557.
- [17] K. A. Olive et al. (Particle Data Group), Chin. Phys. **C38**, 090001 (2014).
- [18] M. Misiak and J. Urban, Phys. Lett. **B451**, 161 (1999), hep-ph/9901278.
- [19] G. Buchalla and A. J. Buras, Nucl. Phys. **B548**, 309 (1999), hep-ph/9901288.
- [20] J. Brod, M. Gorbahn, and E. Stamou, Phys. Rev. **D83**, 034030 (2011), 1009.0947.
- [21] M. Ahmady and R. Sandapen, Phys.Rev.D **88**, 014042 (2013), 1305.1479.
- [22] S. J. Brodsky, G. F. de Teramond, H. G. Dosch, and J. Erlich (2014), 1407.8131.
- [23] J. Beringer et al. (Particle Data Group), Phys.Rev. **D86**, 010001 (2012).
- [24] D. Becirevic, V. Lubicz, F. Mescia, and C. Tarantino, JHEP **0305**, 007 (2003), hep-lat/0301020.
- [25] V. Braun, T. Burch, C. Gatteringer, M. Gockeler, G. Lacagnina, et al., Phys.Rev. **D68**, 054501 (2003), hep-lat/0306006.
- [26] P. Ball, V. M. Braun, and A. Lenz, JHEP **08**, 090 (2007), 0707.1201.
- [27] H.-M. Choi and C.-R. Ji, Phys. Rev. **D75**, 034019 (2007), hep-ph/0701177.
- [28] R. R. Horgan, Z. Liu, S. Meinel, and M. Wingate, Phys. Rev. **D89**, 094501 (2014), 1310.3722.

- [29] W. Altmannshofer, A. J. Buras, D. M. Straub, and M. Wick, JHEP **04**, 022 (2009), 0902.0160.